Available online at www.sciencedirect.com

SciVerse ScienceDirect

Ceramics International 38 (2012) 4653–4659

CERAMICS INTERNATIONAL

www.elsevier.com/locate/ceramint

Glass infiltration of gelcast zirconia-toughened alumina ceramics for dental restoration

Zhengyu Yang [a], Qiong Jin [a,b], Jianfeng Ma [a,b,*], Yiping Tong [a], Xiaofei Wang [a], Ruoxi Du [a,b], Siqian Wang [a,b]

[a] School and Hospital of Stomatology, Wenzhou Medical College, Wenzhou 325027, China
[b] Dental Materials Research Center of Hospital of Stomatology, Wenzhou Medical College, Wenzhou 325027, China

Received 7 February 2012; accepted 11 February 2012
Available online 21 February 2012

Abstract

This study investigated the effects of process parameters and material characteristics in glass infiltration of gelcast zirconia-toughened alumina (ZTA) ceramics for dental applications. Nine types of lanthanum-based silicate glasses with different concentrations of La_2O_3, B_2O_3, and Li_2O were prepared and characterized on the basis of their melting temperature, crystal structure, and thermal characteristics. These glasses were infiltrated into a ZTA matrix that was semi-sintered at 1200 °C to obtain a ceramic material with low shrinkage and high strength. The performance of the glass-infiltrated ceramic samples obtained with various glasses for various infiltration durations and temperatures was evaluated on the basis of the linear shrinkage rate, three-point bending strength, fracture morphology, and elemental composition. From the results, the infiltration temperature was identified as 1150 °C, and the optimum glass composition was 30%La_2O_3–15%Al_2O_3–15%B_2O_3–15%SiO_2–5%Li_2O by mass. The glass-infiltrated gelcast ZTA ceramic has a strength of 291.24 ± 27.94 MPa with a shrinkage of 1.8548 ± 0.2663%. These findings could provide a basis for further development of gelcast dental ceramics, which will make all-ceramic oral restoration less reliant on special equipment and materials.

Keywords: D. Al_2O_3; D. Glass; E. Biomedical applications; Gel casting

1. Introduction

Today, the field of all-ceramic dental restoration is quite mature, and such materials are preferred over porcelain-fused-to-metal crowns because of their better aesthetics and biocompatibility [1,2]. Clinically successful all-ceramic systems in current use include Procera AllCeram®, Vita In-Ceram®, IPS-Empress® 2, Lava™, and Cercon®. However, these systems still have their disadvantages, particularly regarding the energy required in their production and the overall cost implications of the equipment necessary for high-temperature sintering. Furthermore, the outcomes of some of the production processes are strongly dependent on the materials and equipment, such as refractory materials and high-temperature sintering furnaces. These shortcomings, to some extent, do restrict the applications of all-ceramic crowns.

Zirconia-toughened alumina (ZTA) ceramics are widely used in many fields and particularly in dental restorations [3,4] because it exhibits transformation toughening at high temperature, which greatly improves the fracture toughness, strength, and stability [5].

The forming method is the basis of ceramic manufacturing. Commonly, dental all-ceramic crowns are formed by computer-aided design/machining (CAD/CAM) because of the great shrinkage at high temperature. Hence, this technique requires professional-grade equipment and skill as well. For a long fixed bridge of molar teeth, in particular, it is unlikely that an accurate shape can be achieved without computer assistance. To address these limitations, a promising alternative is gelcasting, which is widely established in industrial production as a method that allows simple process control for in situ curing of complex shapes. Furthermore, it is a near

* Corresponding author at: School and Hospital of Stomatology, Wenzhou Medical College, Wenzhou 325027, China. Tel.: +86 0577 88063088; fax: +86 0577 88855488.
E-mail address: dentistmacn@yahoo.com.cn (J. Ma).

0272-8842/$36.00
doi:10.1016/j.ceramint.2012.02.047

net-shape process when semi-sintering is conducted at a low temperature and it affords highly porous microstructures. It is well known that the ceramics can attain a high strength after sintering at high temperature. However, this is based on the densification of ceramic crystals, which may lead to large shrinkage of the green bodies. Glass-infiltrated ceramics, however, do not suffer this problem [2] as they can be sintered at low temperature to avoid great shrinkage, while high strength is attained by infiltrating with glass. Hence, by combining known methods for gelcasting porous ceramics [6–8] with glass infiltration, it would be possible to realize oral ceramic materials with high strength and low shrinkage. The process would require lower amounts of energy and would be less dependent on specific materials and equipment than conventional process, and more significantly, would allow easy manufacture of complex shapes. These advantages would be very significant in clinical applications.

In glass-infiltrated ceramics, the type of glass used plays an important role in determining material performance. Lanthanum-based silicate glasses have excellent strength and chemical stability, and can infiltrate into Al_2O_3 smoothly [9,10]. Moreover, such glasses have good biocompatibility and are therefore, widely studied for the applications to dental restoration [11,12].

However, at present, little is known regarding the effects of glass infiltration on gelcast ZTA ceramics. Hence, the study investigated the feasibility of combining gelcasting with glass infiltration. Specifically, the effects of the glass composition and process parameters (semi-sintering temperature and infiltrating temperature) in the preparation of dental all-ceramic ZTA basal crowns were investigated to obtain high strength and low shrinkage with densification.

2. Materials and methods

2.1. Preparation and characterization of infiltration glasses

To identify a glass composition appropriate for infiltrating the ZTA ceramic matrix, we investigated the impact of different concentrations of La_2O_3, B_2O_3, and Li_2O on the performance of the glass. According to the Tyszblat's patent, nine types of glasses were prepared [2,9,10], as shown in Table 1. Furthermore, 5 wt% ZrO_2 and 2.5 wt% Y_2O_3 was added to the glasses in order to make these elements saturated [13] and avoid chemical reactions between the glass and ZTA.

Glass base powders were prepared according to Table 1 and mixed with pure alcohol. After ball milling for 6 h and drying at 80 °C for 8 h, the glass powders were sintered in a platinum crucible according to the procedure in Fig. 1.

The glasses were characterized on the basis of their melting temperature and by differential thermal analysis (DTA) and X-ray diffraction (XRD) [9,14,15].

The melting temperature was measured on a GFT High-Temperature Contact Angle Analyzer (vacuum environment, Hunan Zhenhua Analysis Instrument Co., Ltd., China). Glass powders were pressed into a cylinder (diameter: 3 mm, length: 4 mm) and placed on the ZTA matrix. Samples were heated at a rate of 5 °C/min and the shape of samples was observed every 5 °C once temperature reached 600 °C. The glass half-spheroidal point temperature and melting temperature were determined, respectively, at the moment when the height of glass specimen reached 75% (3 mm) and 25% (1 mm) of the original [16,17]. Six samples of each type were tested ($n = 6$).

DTA was conducted on an SDTQ600 integrated thermal gravimetric analyzer (ThermoEkmental Inc. America) under

Table 1
Sample compositions and designations for infiltration glasses (mass fraction).

Type	SiO_2	B_2O_3	Al_2O_3	La_2O_3	Li_2O	Y_2O_3	ZrO_2	CaO	TiO_2	CeO_2	Fe_2O_3
La1	20	20	15	20	5	2.5	5	5	5	2	0.5
La2	17.5	17.5	15	25	5	2.5	5	5	5	2	0.5
La4	15	12.5	12.5	35	5	2.5	5	5	5	2	0.5
B2	12.5	20	12.5	30	5	2.5	5	5	5	2	0.5
B3	10	25	10	30	5	2.5	5	5	5	2	0.5
Li	15	20	15	25	5	2.5	5	5	5	2	0.5
Li1	15	15	15	30	5	2.5	5	5	5	2	0.5
Li2	12.5	15	12.5	30	10	2.5	5	5	5	2	0.5
Li3	12.5	10	12.5	30	15	2.5	5	5	5	2	0.5

Fe_2O_3 and CeO_2 were used as glass coloring agent, and TiO_2 was added as a nucleating agent to enhance anticorrosion performance. The Al/Si was kept at 1–1.2 [9] for acquiring a stabilized network of modifier oxides [AlO_6], and CaO was selected as the network adjuster to speed up glass melting.

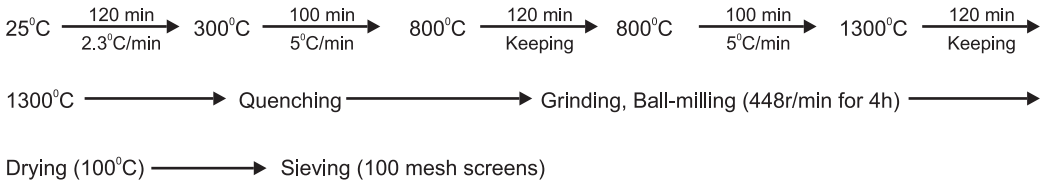

Fig. 1. Glass preparing process.

air atmosphere with Al_2O_3 as the comparison material. The temperature was controlled between 50 °C and 950 °C at a heating rate of 5 °C/min. The phase composition was identified on a D-8 advanced XRD system (Cu K_a radiation; Bruker Inc., Germany), operating at 40 kV and 40 mA with the scanning range from 10° to 90° in steps of 10°/min for 2 h.

2.2. Gelcasting of ZTA composite ceramic

On the basis of previous studies [18–20], a ZTA ceramic matrix was prepared by gelcasting. The premixed liquid comprised deionized water, monomer (Acrylamide, AM, BioDee BioTech Co., Ltd., China), cross-linking agent (*N*,*N*-methylene bisacrylamide, MBAM, BioDee BioTech Co., Ltd., China), and a dispersing agent (SD-07, 0.8 wt%, Xiaoke nano ceramic technology Co., Ltd., China), mass ratio of AM to MBAM was 24:1, and the pH was adjusted to 11 with analytically pure ammonia (Wenzhou Auxiliary Agent Plant, China). To this was added α-Al_2O_3 powder (D_{50} = 0.49 μm, 99.7% purity, Henan Jiyuan Brother Material Co., Ltd., China) and 3Y-ZrO_2 (D_{50} = 30 nm, 99.9% purity, HTNano Material Co., Ltd., China) as the ZTA precursors (4:1 by weight). In addition, 1 wt% MgO (D_{50} = 0.50 μm, 99.6% purity, Zhejiang Hongsheng Technology Co., Ltd.) and 4 wt% TiO_2 (anatase, D_{50} = 5 nm, 99.9% purity, Zhejiang Hongsheng Technology Co., Ltd.) were used as sintering additives. These elements were mixed to obtain a 55 vol% solid concentration gel. After ball milling for 12 h, an initiator (ammonium persulphate, APS, BioDee BioTech Co., Ltd., China) and catalyst (*N*,*N*,*N*′,*N*′-tetramethyl ethylenediamine, TEMED, BioDee BioTech Co., Ltd., China) were ultrasonically mixed into the slurry for 15 s. Subsequently, the degassed slurry was cast into moulds and then in situ polymerized and dried for 48 h to obtain a ceramic green body. Finally, to avoid extraordinary shrinkage, the green body was semi-sintered at 1200 °C (sintering temperature was confirmed to match the glass melting temperature determined previously). After sintering, highly porous ZTA ceramics with a complex three-dimensional microstructure were obtained. A sample of the ZTA matrix (1 mm × 1 mm) was cut and tested on a Micromeritics Auto Pore IV Automatic Mercury Porosimeter to determine the pore size distribution.

2.3. Glass infiltration of ZTA ceramic

The different glasses were infiltrated into ZTA ceramic matrix by the following procedure: The glass powder was mixed with deionised water and then placed on the ceramic surface. This was heated up to 1150 °C at the rate of 5 °C/min. After holding the temperature for 20 min, samples were allowed to cool to below 300 °C and removed from the furnace. Furthermore, because some of the glasses do not infiltrate uniformly [21], samples were infiltrated twice and cut into specimens of size 25 mm × 5 mm × 2 mm. These specimens were subjected to linear shrinkage rate tests, three-point bending strength tests, scanning electron microscope (SEM) analysis of the fracture morphologies, and energy dispersive X-ray spectroscopy (EDS).

The linear shrinkage was calculated as follows:

$$LS\,(\%) = \frac{L_S}{L} \times 100\%$$

where L is the length of the mould (mm), and L_S is the longitudinal shrinkage of the specimen (mm).

The three-point bending strength was determined on an NDN-100 versatile mechanical test machine (KQL Testing Instruments Co., Ltd., China) with a span of 20 mm and a crosshead speed of 0.5 mm/min. Ceramic green body were tested respectively before and after semi-sintering (n = 8), besides, 8 samples were prepared for each glass infiltrated ZTA type. Fracture morphologies of typical tested samples were observed under a JSM-6700F field-emission SEM (JEOL Ltd., Japan). EDS analysis was performed on an INCA 7421 apparatus (The Oxford Instruments Inc, England) to determine the elemental distribution of Si, Ca, Zr, and La between glass and ceramics.

The results were analyzed by factorial ANOVA and Fisher's least significant difference (LSD) t test (α = 0.05, SPSS 13.0)

3. Results and discussion

3.1. Characteristics of ZTA ceramic matrix composite

The three-point bending strength of ZTA ceramic green body reached 33.62 ± 3.54 MPa, 16–24 times higher than those of slip cast and dry pressed bodies [22,23] showing that it can be machined. After semi-sintering at 1200 °C, the strength decreased to 21.52 ± 0.70 MPa. Further, the linear shrinkage was only 0.2882 ± 0.0446%, confirming near net-shape [7], and the porosity was 44.0264%. The pore size (Fig. 2) revealed a single-peak distribution in the range 0.04–0.4 μm. This uniform pore distribution is an excellent advantage of gelcasting, and occurs because AM and MBAM form strong links with ZTA powder in the green body under the influence of dispersing agents. After semi-sintering, these organics volatilize and the uniform pores are obtained. This feature may facilitate glass infiltration.

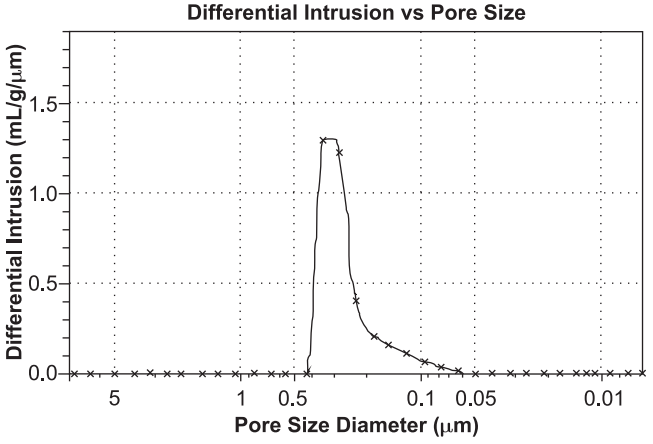

Fig. 2. Pore size distribution of ZTA ceramic after semi-sintering at 1200 °C.

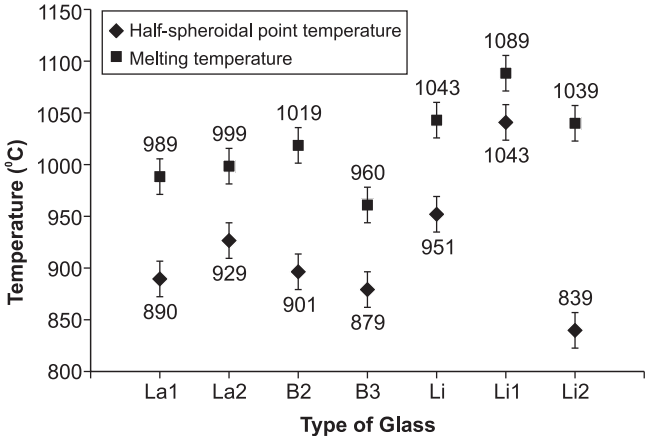

Fig. 3. Melting temperatures of different glass compositions.

3.2. Characteristics of infiltration glasses

The half-spheroidal point temperature and melting temperature are shown in Fig. 3. The high viscosity and low liquidity of types La4 and Li3 prevent the formation of a homogeneous glass. The heights of the specimens did not lower to 2 mm (50% of original) at 1100 °C; hence, these two were eliminated. However, all the other seven did turn into fluids, and the heights of these specimens were all less than 1 mm (25% of original), showing that the seven could fully wet the ZTA ceramic matrix. Thus, despite differences in composition, all glasses had low viscosity and high liquidity and so were suitable to infiltrate the ZTA ceramics. Since the semi-sintering temperature was set to 1200 °C, the infiltration temperature was set to 1150 °C in order to avoid unnecessary shrinkage of the ceramic green body [9,24].

Fig. 4 shows the DTA curves of the seven remaining glasses; here, the temperature of the first endothermic valley is near the glass softening temperature, and the first exothermic peak temperature corresponds to the transition temperature [14,25]. As demonstrated in Fig. 3, the B2 and B3 samples did not show significant endothermic valleys and exothermic peaks, but the other five all had two endothermic peaks. As the B_2O_3 content increased, the melting temperature gradually reduced. That is because B_2O_3, an important network former in the La_2O_3–SiO_2–Al_2O_3–B_2O_3 glass system, can lower the viscosity and raise the chemical stability and impact resistance [15,26–28]. However, an excess of B_2O_3 would result in an abundance of $[BO_3]$ and deficiency of $[BO_4]$, which can degrade the crystallization behavior. This explains why the DTA curves of B2 and B3 did not have obvious exothermic peaks and endothermic valleys.

La^{3+} affects the glass melting temperature and viscosity and improves liquidity at high temperature [15]. Thus, as the La_2O_3 content increased, the DTA curve became flat and the softening temperature and transition temperature decreased. Li^+ encourages melting of quartz crystals, and so the addition of Li can lower glass viscosity and the melting temperature [28]. At temperatures exceeding 618 °C, which is the fusion temperature of lithium carbonate, the fluxing action become even more evident. Thus, the temperature of second endothermic peak for the Li2 samples was significantly lower than that of the other samples, as demonstrated in Fig. 4.

The XRD patterns of the melted glass powders (Fig. 5) confirm that all had an amorphous structure. Samples melted at 1300 °C were fully amorphous [14,29], this suggests that the addition of ZrO_2 and Y_2O_3 to the glass does not produce obvious crystallization with other elements during preparation.

3.3. Characteristics of glass-infiltrated ZTA ceramics formed by gelcasting

On the basis of the results in Tables 2–4, Li1 samples showed the lowest shrinkage of $1.8548 \pm 0.2663\%$ with the highest

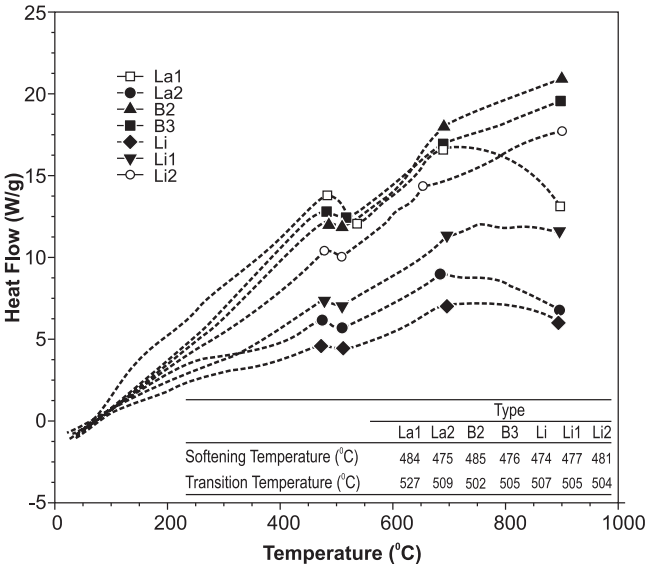

Fig. 4. DTA curves of seven glass compositions that form a homogenous mixture.

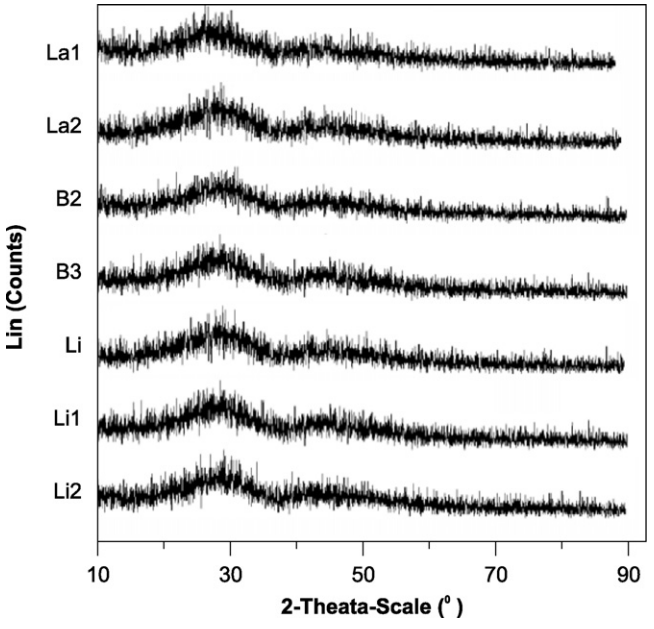

Fig. 5. Diffraction pattern of seven glass compositions melted at 1300 °C.

Table 2
Linear shrinkage rate and three-point bending strengths for seven samples after glass infiltration.

Type	Linear shrinkage rate (%)	Three-point bending strength (MPa)
La1	2.1068 ± 0.0840	258.76 ± 34.92
La2	2.5470 ± 0.0780	207.62 ± 24.33
B2	3.0021 ± 0.1124	197.36 ± 22.00
B3	2.3258 ± 0.2575	245.08 ± 12.56
Li	2.2492 ± 0.2356	207.64 ± 22.03
Li1	1.8548 ± 0.2663	291.24 ± 27.94
Li2	2.0087 ± 0.2410	240.35 ± 24.79

strength of 291.24 ± 27.94 MPa. The statistical analysis showed significant differences ($P < 0.05$) in shrinkage between the Li1 samples and the others (except La1, $P > 0.05$). B2 showed the highest shrinkage of 3.0021 ± 0.1124% with the lowest strength of 197.36 ± 22.00 MPa. Thus, significant differences can be found between B2 and the others in terms of shrinkage ($P < 0.05$). Further, significant differences ($P < 0.05$) were also seen between Li1 and the other samples in terms of the three-point bending strength, and also between B2 and the Li, La1, B3, and Li2 samples. Thus, overall, the Li1 samples displayed lower shrinkage and higher strength, and were chosen as the samples for EDS; B2 samples showed the lowest performance.

As seen in the fracture morphologies in Fig. 6, the semi-sintered ZTA ceramic matrix has a microstructure primarily consisting of obvious pores and a loose structure, while the crystalline grains are well connected. In the La1 samples, the glass infiltrated the ZTA ceramic. However, many pores (white arrows in La1) were still left on the fracture surface. Moreover, although the La2 and B2 samples showed successful infiltration, obvious cracks were found at the contact surface (white arrows in La2 and B2). This may explain the significantly lower strength and higher shrinkage compared with the other glass types. In the B3 samples, the composite ceramic showed evident signs of a disordered microstructure instead of simple infiltration, and the entire field was covered with anomalous stripes. This may be because the content of Al_2O_3 was far from saturation in the glass. Thus, after infiltrating, Al_2O_3 grains were melted into glass, leading to the structural changes. The Li, Li1, and Li2 samples, however, showed good infiltration results. Comparatively speaking, the Li1 samples had the fewest pores, showing that

Table 3
Multiple comparison between each types of linear shrinkage.

Type	La1	La2	B2	B3	Li	Li1	Li2
La1		+	+	−	−	−	−
La2			+	−	+	+	+
B2				+	+	+	+
B3					−	+	+
Li						+	−
Li1							−
Li2							

"+" means there is significant difference between the two types ($P < 0.05$) while "−" means no significant difference exists ($P > 0.05$).

Table 4
Multiple comparison between each types of three-point bending strength.

Type	La1	La2	B2	B3	Li	Li1	Li2
La1		+	+	−	+	+	−
La2			−	+	−	+	+
B2				+	−	+	+
B3					+	+	−
Li						+	−
Li1							+
Li2							

"+" means there is significant difference between the two types ($P < 0.05$) while "−" means no significant difference exists ($P > 0.05$).

the three-dimensional structure of the ZTA ceramic matrix after semi-sintering was almost completely filled with glass. In addition, the infiltrated ceramics exhibited transgranular fracture of Al_2O_3 (white arrow in last image) and lacuna created by grain pullout (black arrow at last image) [30–32].

The Li1 samples, which have less pores and defects into fracture surface, were subjected to EDX analysis at the points shown in Fig. 7. Typically, Si, Ca, and La exist in the glass phase only, but as demonstrated in Fig. 8, these three elements permeated through the ceramic gradually and were even detected at point 5. In addition, the amount of Zr detected at point 1 was far higher than the original content in the glass. This phenomenon suggests that the elements diffused between the ZTA ceramic and glass formed a strong chemical combination [33].

The strength and toughness of ZTA ceramics is reinforced by means of transformation toughening, but the process requires a high sintering temperature of up to 1500 °C. At these temperatures, ceramics are significantly densified, leading to enormous shrinkage of up to 16–20%. For this reason, the performance of all-ceramic dental restorations depends considerably on the materials and equipment. This contributes to the high cost and limited clinical application of these materials. At low temperatures (lower than 1250 °C), because of the high surface energy of nano zirconia and the extensive contact between ZrO_2 and Al_2O_3, ZTA ceramic green bodies undergo some sintering and form an interconnected three-dimensional network. In this study, the ceramic green body has certain strength before sintering because of the use of gelcasting. This stems from the monomer and crosslinking agent, which together with the ZTA powder, form a macromolecular crosslinking structure. Hence, the ceramic green body can be machined completely, and this is very significant in dental applications. After sintering at 1200 °C, the ceramic is not significantly densified because the Al_2O_3 crystalline grains do not grow sufficiently at this temperature. However, the addition of MgO and TiO_2 lower the crystallization temperature of small grains [18,34], allowing nano-ZrO_2 to connect with the Al_2O_3 grains. Therefore, very low shrinkage and high porosity were obtained, allowing the melting glasses to infiltrate into the ceramic matrix via the capillary effect. These features provide the basis for the combination of gelcasting and glass infiltration. As shown in Fig. 6, the abundant pores in the ceramics are filled with glass,

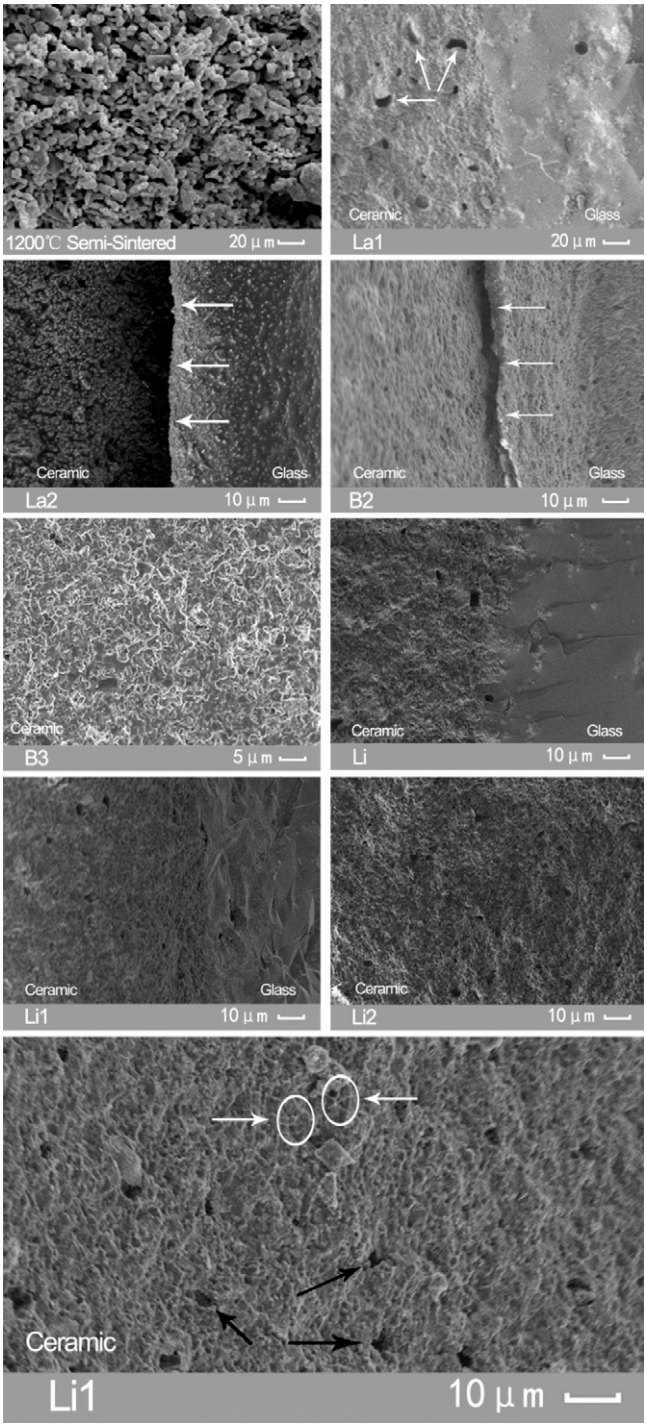

Fig. 6. SEM images of fracture morphologies for different glass-infiltrated samples.

and the two materials support with each other. The network structure limits crack propagation, which explains the considerable improvement in three-point bending strength after infiltration [35,36].

Furthermore, although all the seven types of glass samples could infiltrate ceramic at 1150 °C, differences were still found between them. After infiltration, the La2 and B2 samples displayed a bed joint between glass and ceramic and many pores with different sizes. This suggests these two have many

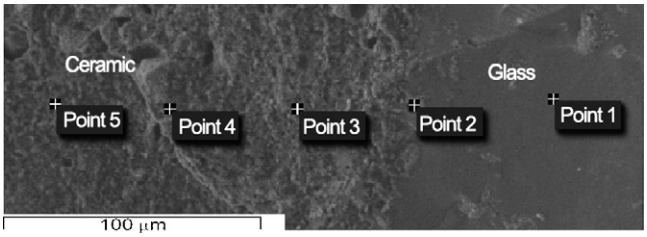

Fig. 7. Micrograph of Li1 sample showing points selected for EDS analysis. The ceramic is toward the left and glass is toward the right. A distance of 25 μm was set between each pair of points. Point 2 is at the interface between the two materials.

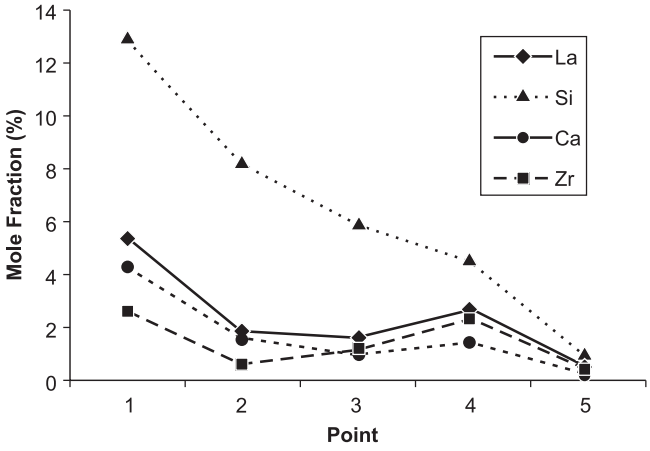

Fig. 8. EDS results for Li1 specimen showing that Si, Ca, and La elements diffuse into the ceramic (points 4 and 5) and an increased Zr content exists at point 1 in the glass.

flaws and do not combine well with ZTA. The other fact is that the La2 and B2 samples showed lower strength and higher shrinkage, which may cause defects during the manufacture and use of dental basal crowns. However, the Li1 samples, including 30%La_2O_3–15%Al_2O_3–15%B_2O_3–15%SiO_2–5%Li_2O (mass fraction), could infiltrate into ZTA matrix with few defects. Moreover, the statistical results indicate that this type of composition has higher strength and lower shrinkage. Hence, this composition is promising for infiltration of ZTA ceramics for dental applications.

Our results show that glass-infiltrated ZTA ceramics formed by gelcasting have reasonable strength and low shrinkage. However, the most important fact is that the ceramic sintering and infiltrating temperatures are all lower than 1200 °C. Hence, there is no need for specialized equipment such as computer-aided design/machining systems to achieve the desired dimensions. In fact, the equipment commonly available to a dental laboratory technician would be sufficient. It is thus clear that the combination of glass infiltration and gelcasting has considerable potential in dental clinical applications.

4. Conclusions

The practicality of dental ZTA all-ceramic restoration materials made by the combination of gelcasting and glass

infiltration was investigated. Our results showed that lanthanum oxide glass can fully infiltrate the ZTA ceramic matrix, and appropriate amounts of B_2O_3 and La_2O_3 can sufficiently lower the softening temperature and transition temperature to facilitate glass infiltration. After semi-sintering at 1200 °C and infiltrating twice with glass powder consisting of 30%La_2O_3–15%Al_2O_3–15%B_2O_3–15%SiO_2–5%Li_2O (mass fraction) at 1150 °C for 20 min, the final glass-infiltrated ZTA ceramic has a near net-shape shrinkage of $1.8548 \pm 0.2663\%$ and reasonable strength of 291.24 ± 27.94 MPa with a dense structure. Thus, the combination of ZTA, gelcasting, and glass infiltration is promising for dental all-ceramic applications and should merit further research.

Acknowledgments

This work is supported by the National Natural Science Foundation of China (grant no. 30870632). Editage provided the editorial and publication support.

References

[1] Y.-Q. Wu, Y.-F. Zhang, G. Pezzotti, J.-K. Guo, Effect of glass additives on the strength and toughness of polycrystalline alumina, J. Eur. Ceram. Soc. 22 (2002) 159–164.
[2] M. Tyszblat, Process for the preparation of a dental prosthesis by slight solid phase fritting of a metal oxide based infrastructure, US Patent, 4,772,434, 1987.
[3] A. Sundh, G. Sjogren, A comparison of fracture strength of yttrium-oxide-partially-stabilized zirconia ceramic crowns with varying core thickness, shapes and veneer ceramics, J. Oral Rehabil. 31 (2004) 682–688.
[4] J. Lalande, S. Scheppokat, R. Janssen, N. Claussen, Toughening of alumina/zirconia ceramic composites with silver particles, J. Eur. Ceram. Soc. 22 (2002) 2165–2171.
[5] X.W. Huang, S.W. Wang, X.X. Huang, Microstructure and mechanical properties of ZTA fabricated by liquid phase sintering, Ceram. Int. 29 (2003) 765–769.
[6] M. Takahashi, R.L. Menchavez, M. Fuji, H. Takegami, Opportunities of porous ceramics fabricated by gelcasting in mitigating environmental issues, J. Eur. Ceram. Soc. 29 (2009) 823–828.
[7] A.C. Young, O.O. Omatete, M.A. Janney, P.A. Menchhofer, Gelcasting of alumina, J. Am. Ceram. Soc. 74 (1991) 612–618.
[8] J. Yang, J. Yu, Y. Huang, Recent developments in gelcasting of ceramics, J. Eur. Ceram. Soc. 31 (2011) 2569–2591.
[9] A. Licciulli, V. Contaldi, S.K. Padmanabhan, A. Balakrishnan, C. Siligardi, D. Diso, Influence of glass phase on Al_2O_3 fiber-reinforced Al_2O_3 composites processed by slip casting, J. Eur. Ceram. Soc. 31 (2011) 385–389.
[10] I. Kratochvilova-Hruba, I. Gregora, J. Pokorny, S. Kamba, Z. Zikmund, J. Petzelt, M. Cernansky, V. Studnicka, V.N. Sigaev, E.N. Smelyanskaya, Vibrational spectroscopy of $LaBSiO_5$ glass and glass–crystal composites, J. Non-Cryst. Solids 290 (2001) 224–230.
[11] Y.F. Yi, N. Wen, H.C. Liu, J.M. Tian, The influence of different metal oxides on the color of dental glass infiltration alumina ceramics, Rare Metal Mater. Eng. 36 (2007) 79–81.
[12] V.B.B. Pinto, P.T.G. Silva, M.V.R. Bica, M.C.S. Nobrega, T. Ogasawara, Micrographic characterization of La-glass infiltrated ZTA bars and its correlation to the three-point flexural strength, Materia 13 (2008) 617–623.
[13] L.D. Yong, J. Ju-Woong., K. Bae-Yeon., Effect of zirconia addition on mechanical and optical properties of alumina/zirconia-glass composites prepared by melt infiltration, J. Mater. Sci. Lett. 22 (2003) 1451–1454.
[14] J. Banjuraizah, H. Mohamad, Z.A. Ahmad, Effect of melting temperatures on the crystallization and densification of $2.8MgO{\cdot}1.5Al_2O_3{\cdot}5SiO_2$ glass-ceramic synthesized from mainly talc and kaolin, J. Alloys Compd. 509 (2011) 1874–1879.
[15] I. Dyamant, E. Korin, J. Hormadaly, Thermal and some physical properties of glasses in the La_2O_3–CaO–B_2O_3 ternary system, J. Non-Cryst. Solids 354 (2008) 3135–3141.
[16] J.H. Shi, W.Q. Chen, M.M. Zhang, Q. Li, H.G. Zheng, Study on melting temperature of AOD slag, Chin. Metall. 17 (2007) 41–45.
[17] Y.Q. Sun, Q.Z. Chen, J.Y. Hu, J.Q. Pan, Study on melting property experiment of BaO–CaO–CaF_2–Cr_2O_3 slag system, J. Shanghai Inst. Technol. 5 (2005) 117–124.
[18] J.F. Ma, S.Q. Wang, R.X. Du, X.D. Li, Pressureless sintering of gelcast ZTA-MgO–TiO_2 systems as potential dental ceramics, Adv. Appl. Ceram. 110 (2011) 275–279.
[19] J. Ma, K. Zhao, B. Shi, X.D. Zhang, Y. Chao, X.D. Li, Preparation of nano-ceramic composite as dental prosthetic material, Key Eng. Mater. 342–343 (2007) 645–648.
[20] J. Ma, K. Zhao, C. Liu, D. Zhang, X.D. Zhang, Y. Chao, X.D. Li, Composition optimization of zirconia toughened alumina for dental ceramics, Key Eng. Mater. 330–332 (2007) 1369–1372.
[21] B.R. Marple, D.J. Green, Mullite alumina particulate composites by infiltration processing: II, Infiltration and characterization, J. Am. Ceram. Soc. 73 (1990) 3611–3616.
[22] J.S. Ha, Effect of atmosphere type on gelcasting behavior of Al_2O_3 and evaluation of green strength, Ceram. Int. 26 (2000) 251–254.
[23] R. Gilissen, J.P. Erauw, A. Smolders, E. Vanswijgenhoven, J. Luyten, Gelcasting a near net shape technique, Mater. Des. 21 (2000) 251–257.
[24] R.V. Mangalaraja, B.K. Chandrasekhar, P. Manohar, Effect of ceria on the physical, mechanical and thermal properties of yttria stabilized zirconia toughened alumina, Mater. Sci. Eng. A: Struct. Mater. Prop. Microstruct. Process. 343 (2003) 71–75.
[25] J.M. Rincon, M. Romero, A. Hidalgo, M.J. Liso, Thermal behaviour and characterization of an iron aluminum arsenate mineral: mansfieldite-scorodite series, J. Therm. Anal. Calorim. 76 (2004) 903–911.
[26] M.I. Ojovan, K.P. Travis, R.J. Hand, Thermodynamic parameters of bonds in glassy materials from viscosity – temperature relationships, J. Phys.: Condens. Matter 19 (2007).
[27] X.M. Shi, Q. Wang, C.X. Li, X.J. Niu, F.P. Wang, K.Q. Lu, Densities of Li_2O–B_2O_3 melts, J. Cryst. Growth 290 (2006) 637–641.
[28] S. Fujino, C.W. Hwang, K. Morinaga, Density, surface tension, and viscosity of PbO–B_2O_3–SiO_2 glass melts, J. Am. Ceram. Soc. 87 (2004) 10–16.
[29] H. Brequel, J. Parmentier, G.D. Sorar, L. Schiffini, S. Enzo, Study of the phase separation in amorphous silicon oxycarbide glasses under heat treatment, Nanostruct. Mater. 11 (1999) 721–731.
[30] K.-H. Chong, J. Chai, Y. Takahashi, W. Wozniak, Flexural strength of in-ceram alumina and in-ceram zirconia core materials, Int. J. Prosthodont. 15 (2002) 183–188.
[31] W.D. Wolf, K.J. Vaidya, L.F. Francis, Mechanical properties and failure analysis of alumina-glass dental composites, J. Am. Ceram. Soc. 79 (1996) 1769–1776.
[32] H. Honlberger, P.M. Marquis, S. Christiansen, H.P. Strunk, Microstructure of a high strength alumina glass composite, J. Mater. Res. 11 (1996) 855–858.
[33] M.G. Rasteiro, T. Gassman, R. Santos, E. Antunes, Crystalline phase characterzation of glass–ceramic glazes, Ceram. Int. 33 (2005) 305–309.
[34] K.A. Berry, M.P. Harmer, Effect of MgO solute on microstructure development in Al_2O_3, J. Am. Ceram. Soc. 69 (1986) 143–149.
[35] Y. Sakka, D.D. Bidinger, I.A. Aksay, Processing of silicon carbide–mullute–alumuna nanocomposites, J. Am. Ceram. Soc. 78 (1995) 479–486.
[36] K. Wang, M.D. Sacks, Mullite formation by endothermic reaction of α-Al_2O_3/silica microcomposite particles, J. Am. Ceram. Soc. 79 (1996) 12–16.